

# Coherent Structures in Scalar Feed-Forward Chains

Christopher Browne\* & Andrew L. Dickerson†

Sponsors: Grégory Faye‡ & Arnd Scheel§

## Abstract

We study semi-infinite and bi-infinite scalar feed-forward networks. We find that the temporal dynamics of these systems is closely linked to the spatial dynamics of an associated interval map and show how this interval map may be used to describe stationary interfaces. Beyond stationary structures, we show that the onset of instabilities in finite networks is intimately related to the emergence of frustrated invasion fronts. These concepts are then applied to several toy models, whose intracellular dynamics mimic the normal form of elementary steady-state bifurcations.

## 1 Introduction

We study coherent structures in scalar feed-forward networks in a systematic fashion. We focus on linear, nearest-neighbor coupling, and find that the use of spatial dynamics allows for an almost complete classification of coherent structures. Being more precise, we study systems of form

$$\dot{u}_j = f(u_j) + \alpha(u_j - u_{j-1}), \quad j \geq 1, \quad (1.1a)$$

$$\dot{u}_0 = f(u_0), \quad (1.1b)$$

where  $u_j \in \mathbb{R}$ . We will also extend our analysis to bi-infinite chains where we will take  $j \in \mathbb{Z}$ . Throughout this paper, we explore three types of nonlinearities,

- *fold*:  $f(u) = 1 - u^2$ ;
- *pitchfork*:  $f(u) = u(1 - u^2)$ ;
- *cusp*:  $f(u) = u(1 - u)(u - a)$ ,

which govern the intracellular dynamics of our system. In the first two examples, we are mostly interested in the competition between stable and unstable states. We study the cubic nonlinearity (cusp) in order to explore competition between different stable equilibria.

---

\*Department of Mathematical Sciences, Rensselaer Polytechnic Institute. Email: brownc12@rpi.edu

†Department of Mathematics, University of Wisconsin-Madison. Email: aldickerson@wisc.edu

‡School of Mathematics, University of Minnesota. Email: gfaye@umn.edu

§School of Mathematics, University of Minnesota. Email: scheel@umn.edu

One may interpret the system (1.1) as the discretization of the simple advection equation

$$\partial_t u = f(u) + \text{sgn}(\alpha) \partial_x u.$$

However, this interpretation is only appropriate for  $\alpha < 0$ ,  $|\alpha| \gg 1$ . For  $\alpha > 0$ , the discretization is ill-posed and generates numerical oscillations, which will manifest as “flip flops”, in our network. For  $|\alpha| \ll 1$ , one expects to see discretization effects, with a plethora of solutions. In fact, one readily notices that for  $\alpha = 0$ , all equations decouple, and the set of stationary solutions is isomorphic to  $\{f^{-1}(0)\}^{\mathbb{Z}}$ .

Our main motivation comes from recent work in [5] and, more specifically, [8]. In these articles, bifurcations in coupled cell networks are studied systematically, exploiting normal form transformations in the presence of specific network structures to give predictions for dynamics near instabilities. One of the most striking observations is the fact that bifurcations lead to solutions exhibiting a rapid growth in amplitude as a function of cell index. For instance, Hopf bifurcations lead to amplitudes  $\mu^{\frac{1}{2} \frac{1}{3j-1}}$  at cell position  $j$ , where  $\mu$  represents a principal bifurcation parameter. The semi-infinite feed-forward network therefore acts as an effective amplifier of the input dynamics in cell  $j = 0$  (which is of course independent of the dynamics in cells  $j > 0$ ). The particular dynamics at cell  $j = 0$  are motivated by the presence of “symmetries”, which require dynamics in all cells to be identical in the sense that the same number of inputs is received. In this sense, the input  $u_{j-1}$  is replaced by  $u_j$  for cell  $j = 0$ , leading to a cancellation and vanishing of the coupling term  $\alpha(u_j - u_{j-1})$ .

The rapid growth of equilibrium amplitudes with  $j$  also points to limitations of a local bifurcation analysis. In particular, one expects that the expansions of these quantities are only valid for extremely small parameter values  $\mu$ , i.e. as long as  $\mu^{\frac{1}{2} \frac{1}{3j-1}} \ll 1$ .

Our main objective is to elucidate this phenomenon and provide a conceptual analysis beyond the limitations of a local analysis for specific models. Our first main observation is that the instability studied in [8] can be understood as a transition from a convective to an absolute instability [1, 7, 11]. In the “stable” regime, perturbations grow in amplitude but are transported along the lattice so that they decay at any fixed initial location  $j$ . The speed of transport  $c$  decreases as the parameter approaches a critical value, at which point stationary solutions bifurcate. The instability can therefore be understood as the transition from a receding invasion front to a stationary interface. In other contexts, the emerging stationary interfaces that typically connect the unstable state to a large, finite-amplitude state at the end of the lattice  $j \rightarrow \infty$ , are often referred to as nonlinear global modes [2, 4].

We analyze this transition in detail and uncover how the receding invasion front picks up an increasingly rapid exponential decay as the speed converges to zero. This steepening of the front can be understood as a precursor to the existence of stationary profiles exhibiting a rapid growth in amplitude with  $j$ . Mathematically, this steep decay mirrors the disappearance of a double root at infinity in the complex plane. Intuitively, exponential, temporal growth generated by the instability becomes sufficiently strong to compensate for the effective transport towards increasing  $j$  and would, in a non-feed-forward situation, lead to transport towards  $j = -\infty$ , that is, negative speeds would emerge. Clearly, such transport is prohibited by our

network structure, where cells of index  $j_*$  simply ignore cell dynamics at  $j > j_*$ . Thus, we will see the formation of frustrated invasion fronts precisely when this transition occurs.

Beyond these stable-unstable interfaces responsible for transitions from convective to absolute instability, we study existence and stability of more general interfaces between stable states in the system. We choose to focus on interfaces between the most interesting (and from a numerical discretization point of view most dangerous) of these stable states, namely, spatially homogeneous,  $j$ -independent, states and period-two states. Our main contribution is a simple criterion that gives stability information and existence of interfaces based on readily computable properties of an interval map for spatial dynamics. We also illustrate the effectiveness of these criteria in a systematic numerical exploration of parameter space.

The remainder of this paper is organized as follows. Section 2 contains our main general results on stability of period-two equilibria and existence of interfaces, independent of the specific shape of  $f$ . Section 3 contains the analysis of fold and pitchfork, including spreading speed calculations. Section 4 treats the more complex case of the cusp.

## 2 Coherent Structures and Interval Maps

The core of this section is the relationship between the existence of stationary interfaces, i.e. temporally stable network configurations, and dynamics of an interval map produced from (1.1). Throughout the remainder of this section, we will ignore the first node in our network (though we will later comment on the effects of this truncation), and extend our analysis to a bi-infinite chain,

$$\dot{u}_j = f(u_j) + \alpha(u_j - u_{j-1}), \quad \forall j \in \mathbb{Z}, \quad \alpha \neq 0. \quad (2.1)$$

### 2.1 Equilibria and Stability

Seeking a method to compute the values of the temporal equilibria of each subsequent cell in our system, we set  $\dot{u}_j = 0$  in (2.1), producing the one-term backward recursion

$$u_{j-1}^* = g(u_j^*) := u_j^* + \frac{f(u_j^*)}{\alpha}. \quad (2.2)$$

Throughout this paper, we will consistently differentiate between the temporal dynamics of our system, related to (2.1), and the spatial (in  $j$ ) dynamics of our system corresponding to the sequence  $(u_j^*)_{j \in \mathbb{Z}}$ , the orbit under  $g$  of our temporal steady states.

**Lemma 2.1.** *Spatially homogeneous ( $j$ -independent) equilibria  $u_j^* \equiv \bar{u}$ ,  $j \in \mathbb{Z}$  of (2.1) are given precisely by the zeros of  $f$ . These equilibria are linearly asymptotically stable for our temporal dynamics precisely when they are linearly unstable for the spatial dynamics (when  $|g'(\bar{u})| > 1$ ) and when  $\alpha g'(\bar{u}) < 0$ .*

**Proof.** It suffices to show that the spectrum of the bi-infinite matrix obtained by linearizing (2.1) is strictly contained in the left hand side of the complex plane precisely when  $|g'(\bar{u})| > 1$  and  $\alpha g'(\bar{u}) < 0$ . To this end, we employ a Fourier transform,  $u_j(t) = \hat{u}_\nu(t)e^{ij\nu}$  to change our linearization

$$\dot{u}_j = f'(\bar{u})u_j + \alpha(u_j - u_{j-1}), \quad j \in \mathbb{Z},$$

into

$$\dot{\hat{u}}_\nu e^{ij\nu} = f'(\bar{u})\hat{u}_\nu e^{ij\nu} + \alpha (\hat{u}_\nu e^{ij\nu} - \hat{u}_\nu e^{ij\nu} e^{-i\nu}), \quad j \in \mathbb{Z}. \quad (2.3)$$

Upon substitution of the ansatz  $\hat{u}_\nu(t) = e^{\lambda t}$  into (2.3), we find the dispersion relation

$$\lambda(\nu) = f'(\bar{u}) + \alpha(1 - e^{-i\nu})$$

We see that for  $\alpha > 0$  we will have  $\Re(\lambda(\nu)) < 0$  precisely when  $f'(\bar{u}) + 2\alpha < 0$ , while for  $\alpha < 0$ , we will require  $f'(\bar{u}) < 0$ . Recalling (2.2), we see that

$$f'(\bar{u}) = \alpha(g'(\bar{u}) - 1). \quad (2.4)$$

Thus, we see that for  $\alpha > 0$ ,  $f'(\bar{u}) + 2\alpha < 0$  precisely when  $g'(\bar{u}) < -1$ , while for  $\alpha < 0$ ,  $f'(\bar{u}) < 0$  precisely when  $g'(\bar{u}) > 1$ . Then noting that our condition  $\alpha g'(\bar{u}) < 0$  effectively forces  $g'(\bar{u})$  and  $\alpha$  to be of opposite sign, we see that for  $\alpha > 0$ ,  $g'(\bar{u}) < 0$ , while for  $\alpha < 0$ ,  $g'(\bar{u}) > 0$ . This, together with the conditions discussed in the previous paragraph, ensures that we will have  $\Re(\lambda) < 0$  precisely when  $|g'(\bar{u})| > 1$  and  $\alpha g'(\bar{u}) < 0$ , from which the result follows. ■

We now turn our attention to describing period-two solutions of (2.2), which we will refer to as "flip flops".

To compute explicitly these period two equilibria, we reduce (2.1) to the system

$$\dot{u}_0 = f(u_0) + \alpha(u_0 - u_1), \quad (2.5a)$$

$$\dot{u}_1 = f(u_1) + \alpha(u_1 - u_0). \quad (2.5b)$$

Equilibrium solutions of this period-two chain,  $u_0 = u_{\text{flip}}, u_1 = u_{\text{flop}}$  will themselves be equilibria on our bi-infinite lattice, that is,  $u_{2j} = u_{\text{flip}}, u_{2j+1} = u_{\text{flop}}, j \in \mathbb{Z}$  will constitute an equilibrium solution of (2.1).

**Lemma 2.2.** *A non homogeneous, period two equilibrium of (2.1),  $u_0 = u_{\text{flip}}, u_1 = u_{\text{flop}}$ , is linearly stable in our temporal dynamics precisely when  $|G'(u_f)| > 1$  and  $\alpha g'(u_f) < 0$  for both  $u_f = u_{\text{flip}}$  and  $u_f = u_{\text{flop}}$ , where  $G = g \circ g$ .*

**Proof.**

From our definition of  $G$ , we note that

$$G'(u_{\text{flip}}) = g'(u_{\text{flip}})g'(g(u_{\text{flip}})) = g'(u_{\text{flip}})g'(u_{\text{flop}}) = g'(g(u_{\text{flop}}))g'(u_{\text{flop}}) = G'(u_{\text{flop}}). \quad (2.6)$$

So, we will have both  $|G'(u_{\text{flip}})| > 1$  and  $|G'(u_{\text{flop}})| > 1$  precisely when  $|g'(u_{\text{flip}})g'(u_{\text{flop}})| > 1$ .

To begin, we set  $u_{2j} = v_j, u_{2j+1} = w_j$ , and rewrite the linearization of our system (2.1) about our equilibrium  $(u_{\text{flip}}, u_{\text{flop}})$ ,

$$\dot{v}_j = f'(u_{\text{flip}})v_j + \alpha(v_j - w_{j-1}) \text{ and } \dot{w}_j = f'(u_{\text{flop}})w_j + \alpha(w_j - v_j).$$

Substituting  $v_j(t) = \hat{v}_\nu(t)e^{-ij\nu}$ ,  $w_j(t) = \hat{w}_\nu(t)e^{-ij\nu}$  into the above equations we obtain the Jacobian matrix

$$J(\nu) = \begin{pmatrix} f'(u_{\text{flip}}) + \alpha & -\alpha e^{-i\nu} \\ -\alpha & f'(u_{\text{flip}}) + \alpha \end{pmatrix}, \quad (2.7)$$

where  $\nu \in [0, 2\pi]$ . We note that the trace of this matrix is independent of  $\nu$  and real.

- We first assume temporal stability of our equilibrium. Thus we must have that the real part of the eigenvalues associated with  $J(\nu)$  are strictly negative for all  $\nu \in [0, 2\pi]$ . In particular, at  $\nu = 0$ , we must have both  $\det(J(0)) > 0$ , and  $\text{tr}(J) < 0$ . Noting that we may rewrite  $\det(J(0))$  as

$$\det(J(0)) = \alpha^2 \left( \left( \frac{f'(u_{\text{flip}})}{\alpha} + 1 \right) \left( \frac{f'(u_{\text{flip}})}{\alpha} + 1 \right) - 1 \right). \quad (2.8)$$

We see that by using (2.4), we may rewrite our condition  $\det(J(0)) > 0$

$$\det(J(0)) = g'(u_{\text{flip}})g'(u_{\text{flip}}) = G'(u_{\text{flip}}) > 1, \quad (2.9)$$

and so  $|G'(u_{\text{flip}})| > 1$ .

Then, noting that we may rewrite  $\text{tr}(J(0)) < 0$  as

$$(\alpha g'(u_{\text{flip}})) + (\alpha g'(u_{\text{flip}})) < 0$$

and that  $\alpha g'(u_{\text{flip}})\alpha g'(u_{\text{flip}}) > 0$ , we immediately see that both  $\alpha g'(u_{\text{flip}})$  and  $\alpha g'(u_{\text{flip}})$  are negative. Thus,  $\text{tr}(J) < 0$ .

- Now reversing directions, and keeping in mind that the assumptions  $\alpha g'(u_f) < 0$  and  $|G'(u_f)| > 1$  for  $u_f = u_{\text{flip}}$ ,  $u_f = u_{\text{flip}}$  are equivalent to the conditions  $\text{tr}(J) < 0$  and  $\det(J(0)) > 0$ , we will proceed to show temporal stability of our solution by showing that for all  $\nu \in [0, 2\pi]$ ,

$$\Re(\lambda_{\pm}(\nu)) = \frac{\text{tr}(J)}{2} \pm \Re\left(\sqrt{D(\nu)}\right) < 0,$$

where

$$D(\nu) = \frac{\text{tr}^2}{4} - \det(J(\nu)) = \left( \frac{f'(u_{\text{flip}}) - f'(u_{\text{flip}})}{2} \right)^2 + \alpha^2 e^{-i\nu}$$

denotes the discriminant of  $J(\nu)$ . As we are already have that  $\Re(\lambda_{\pm}(0)) = \lambda_{\pm}(0) < 0$ , it will suffice to show that

$$\Re\left(\sqrt{D(\nu)}\right) < \sqrt{D(0)}, \quad \forall \nu \in [0, 2\pi]. \quad (2.10)$$

Writing  $D(\nu) = A + Be^{-i\nu}$ ,  $A, B > 0$ , we begin by rewriting (2.10) as

$$\sqrt{A + Be^{i\nu}} + \sqrt{A + Be^{-i\nu}} < 2\sqrt{A + B}, \quad \forall \nu \in [0, 2\pi]. \quad (2.11)$$

Taking without loss of generality  $A = 1$ , and squaring both sides of (2.11), we find the positive, real, relation

$$2 + 2B \cos(\nu) + 2\sqrt{1 + B^2 + 2B \cos(\nu)} < 4 + 4B$$

which is equivalent to the obviously valid relation

$$1 + B^2 + 2B \cos(\nu) < \frac{(2 + 2B(2 - \cos(\nu)))^2}{4} = 1 + B^2(2 - \cos(\nu))^2 + 2B(2 - \cos(\nu)).$$

Thus for all  $\nu \in [0, 2\pi]$  we have  $\Re(\sqrt{D(\nu)}) < \sqrt{D(0)}$ , and so  $\Re(\lambda_{\pm}(\nu)) < 0$ . Thus, our equilibrium is temporally stable. ■

**Remark 2.3.** *In later sections, where we discuss the temporal and spatial stability of particular equilibria for specific  $f$ , it will suffice to consider only the case  $\nu = 0$ , as we have shown that stability in this case will imply stability  $\forall \nu \in [0, 2\pi]$ .*

**Corollary 2.4.** *Period-two equilibria are temporally stable precisely when they are stable in a period-two chain, that is, when  $j \in \mathbb{Z}/(2\mathbb{Z})$ .*

**Remark 2.5.** *While higher period solutions to (2.1) may exist, we will examine only homogeneous and flip flop solutions. When  $\alpha = 0$ , we see that the set of equilibria of (2.1) is isomorphic to  $\{f^{-1}(0)\}^{\mathbb{Z}}$ . We will not attempt to describe how this plethora of solutions evolves as  $|\alpha|$  is increased.*

## 2.2 Stationary Interfaces

We now define our first coherent network structure in terms of heteroclinic connections, which we will refer to as a stationary profile, as follows. A heteroclinic connection between two equilibria is a spatial trajectory,  $(u_j)_{j \in \mathbb{Z}}$ , joining  $u_+$  at  $j = \infty$ , and  $u_-$  at  $j = -\infty$ . We will also consider heteroclinic connections to flip flop equilibria, i.e.  $|u_{2j} - u_{\text{flip}}| + |u_{2j+1} - u_{\text{flop}}| \rightarrow 0$  as  $j \rightarrow \infty$ . We say that a stationary profile exists between two states,  $A$  at  $j = -\infty$  and  $B$  at  $j = \infty$ , if and only if such a heteroclinic connection exists between these two states. Throughout this paper, we will use the notation  $A \rightarrow B$ , to denote the existence of a stationary profile between  $A$  and  $B$ . Further, the notation  $FF \rightarrow B$ , will denote a stationary profile whose left hand side (at  $j = -\infty$ ) is a flip flop equilibrium.

**Lemma 2.6.** *Let the state  $\bar{u}$  at  $j = -\infty$  be stable for the temporal dynamics of our system. Then, a heteroclinic cannot exist if there does not exist  $u_p \neq \bar{u}$  such that  $g(u_p) = \bar{u}$ . Similarly, heteroclinic connections to flip flops,  $\bar{u}_{\text{flip}}, \bar{u}_{\text{flop}}$  as  $j = -\infty$  cannot exist when there exists no  $u_p \notin \{\bar{u}_{\text{flip}}, \bar{u}_{\text{flop}}\}$ , such that  $g(u_p) = \bar{u}_{\text{flip}}$  or  $g(u_p) = \bar{u}_{\text{flop}}$ .*

**Proof.** Let  $\bar{u}$  denote a temporally stable equilibrium solution at  $j = -\infty$ , whose only preimage under  $g$  is  $\bar{u}$ , but with  $u_j \rightarrow u_p$  as  $j \rightarrow \infty$ . By Lemma 2.1, this cannot happen, as a temporally stable state must be unstable for our spatial,  $g$ , dynamics, and so  $\bar{u}$  is a repeller for our map  $g$ . ■

**Remark 2.7.** *There do not exist heteroclinic connections to a temporally unstable state at  $j = \infty$ , as these states are stable for our map  $g$  by Lemma 2.1, and therefore there exist no trajectories converging to them in backward spatial iteration.*

**Lemma 2.8.** *In semi-infinite networks, i.e., when  $0 \leq j < N, N = \infty$ , the conditions of Lemma 2.6 may be extended to include temporally unstable states at  $j = 0$ .*

**Proof.** Let the state  $\bar{u}_1$  be a temporally unstable solution at  $j = 0$ , whose only preimage under  $g$  is  $\bar{u}_1$ . Let  $\bar{u}_2$  denote an equilibrium solution at  $j = \infty$ ,  $\bar{u}_1 \neq \bar{u}_2$ . If a heteroclinic connection existed between the two states in question, it would follow that there exists  $u_p \neq \bar{u}_1$  such that,  $g^{-1}(u_p) \neq \bar{u}_1$ , which is clearly a contradiction. ■

**Remark 2.9.** *In semi-infinite networks, there exists a heteroclinic connection between the state  $A$  at  $j = 0$  and  $B$  at  $j = \infty$  if and only if there exists a preimage  $u_p$  such that  $g(u_p) = A$  and the subsequent preimages of  $u_p$ ,  $g^{-j}(u_p), j \in \mathbb{Z}^+$  satisfy  $g^{-j}(u_p) \rightarrow B$  as  $j \rightarrow \infty$ .*

**Remark 2.10.** *If there exists a stationary profile in a semi-infinite network, then there exists an analogous stationary profile in an infinite network.*

### 2.3 Moving Interfaces: Propagation into Unstable States

Taking motivation from the original bifurcation studies of [8] carried out in finite networks, we focus on describing possible bifurcations on our infinite lattice, corresponding to the transition between convective and absolute spreading of instabilities through our network.

To find these bifurcation points, we will attempt to describe the speed at which instabilities propagate from cell to cell. Knowing from [10] that these speeds may be computed by examining the linear speed of propagation away from the unstable state,  $\bar{u}$ , subject to a small perturbation, we linearize our system (2.1) about  $\bar{u}$  giving

$$\dot{u}_j = f'(\bar{u})u_j + \alpha(u_j - u_{j-1}).$$

We then employ the Fourier Transform  $u_j = e^{\lambda t} e^{-i(j-ct)\sigma}$ , (where  $\sigma$  may be complex) to obtain the dispersion relation  $d(\lambda, i\sigma) = \lambda + f'(\bar{u}) + \alpha(1 - e^{-i\sigma})$ . We may then use the double root conditions

$$d(ic\sigma, i\sigma) = 0, \tag{2.12a}$$

$$\partial_2 d(ic\sigma, i\sigma) = 0 \tag{2.12b}$$

to find our spreading speeds.

In general, we find that equations (2.12) have at most two solutions,  $c_1, c_2$ . Further, we find that the precise moment of transition from convective to absolute spreading of instability coincides with the moment at which one of our speeds becomes 0, and then vanishes.

**Remark 2.11.** *In a network with initial condition  $u_j = A$  for  $j \leq j^*$ ,  $A$  stable and  $u_j = B$  for  $j > j^*$ ,  $B$  unstable, the speed at which the state  $A$  "invades"  $B$  will be given by  $c = \max\{c_1, c_2\}$ ; see [10] for details.*

**Remark 2.12.** *By definition of our network coupling, negative wavespeeds will not be possible. This means that a stable state cannot invade an unstable state to the left, leading to the presence of what we will call "Frustrated Invasion Fronts", whose propagation is blocked by our network structure.*

Beyond our linear analysis, one may consider nonlinear front solutions. There typically exists a one-parameter family of such fronts and the steepest front is selected by compactly supported initial conditions. Existence of such fronts leads to delay equations rather than the map  $g$  and has been studied with slightly different objectives in [6]. Similarly, information about traveling fronts that connect stable equilibria also leads to delay equations and is beyond the scope of this article.

### 3 Fold and Pitchfork Bifurcations

In this section, we examine the two specific nonlinearities,  $f(u) = 1 - u^2$ , and  $f(u) = u(1 - u^2)$ , associated with the normal forms of the saddle node and pitchfork bifurcations respectively. We will later see that by understanding the dynamics of this system, we gain valuable insight into more complicated dynamics such as the nonlinearity associated with the normal forms of the cusp bifurcation.

#### 3.1 Fold Bifurcation

##### 3.1.1 Temporal Stability of Steady States

Letting  $f(u) = 1 - u^2$ , we begin by characterizing the conditions on  $\alpha$  which will permit the existence and temporal stability of various period-two (i.e. homogeneous and flip flop) equilibria of (2.1).

**Lemma 3.1.** *There exist precisely two homogeneous equilibria of our system corresponding to the states  $-1$  and  $1$ . For  $|\alpha| < 1$ , there also exists one flip flop equilibrium given by  $u_{2j} \equiv \alpha + \sqrt{1 - \alpha^2}$  and  $u_{2j+1} \equiv \alpha - \sqrt{1 - \alpha^2}$ , for all  $j \in \mathbb{Z}$ . Furthermore, we find that the states  $-1$  and flip flop are always temporally unstable, while  $1$  is temporally stable provided  $\alpha < 1$ .*

**Proof.** Our desired result follows by a simple application of Remark 2.3 and Corollary 2.4. To verify, for instance, the stability of our flip flop equilibrium, we inspect the Jacobian of our 2-cell system

$$J(0) = \begin{pmatrix} f'(u_0) + \alpha & -\alpha \\ -\alpha & f'(u_1) + \alpha \end{pmatrix},$$

from which we derive the eigenvalues associated with our flip flop equilibrium,

$$\lambda_{\text{ff}\pm} = -\alpha \pm \sqrt{4 - 3\alpha^2}$$

Noting that for  $|\alpha| < 1$ ,  $\lambda_{\text{ff}+} > 0$ , temporal instability follows. ■

### 3.1.2 Stationary Interfaces

Considering both semi-infinite and bi-infinite length chains, we now discuss the existence of stationary interfaces in our network. We know from Remark 2.7 that we can expect to observe at most two stationary interfaces in our system, each of form  $-1 \rightarrow 1$  and  $FF \rightarrow 1$  respectively. Further, since 1 is stable only when  $\alpha < 1$ , and since flip flops only exist for  $|\alpha| < 1$ , we already have upper bounds on the region of existence for these structures.

**Lemma 3.2.** *We find for semi-infinite networks that stationary profiles of form  $-1 \rightarrow 1$  exist precisely for  $-2 < \alpha < 1$ , while for bi-infinite networks, such a profile exists for  $\alpha < 1$ . Stationary profiles of form  $FF \rightarrow 1$  exist for  $|\alpha| < 1$  in both semi-infinite and bi-infinite networks.*

**Proof.** Here we use Remarks 2.9 and 2.10 to derive conditions on  $\alpha$  which will permit the existence of various stationary profiles. Here we will show only the methods by which we determine the conditions on  $\alpha$  which allow a stationary interface between the states  $-1$  and  $1$ . The same methods are used to uncover these regions for  $FF \rightarrow 1$  stationary profiles. To determine the bounds of existence for stationary profiles of form  $-1 \rightarrow 1$ , we examine case by case the preimages of  $-1$  under  $g$  for various  $\alpha$ .

- $0 < \alpha < 1$  : With our just mentioned remarks in mind, we note that in this parameter regime, there exists  $u_p \neq -1$  such that  $g(u_p) = -1$ . Further, subsequent preimages of  $u_p$  converge to  $1$  as  $j \rightarrow \infty$ , and so we conclude for both semi-infinite and bi-infinite networks that a  $-1 \rightarrow 1$  stationary profile exists.
- $-2 < \alpha < 0$  : Here, we find precisely the same behavior as in the previous region, and thus arrive at the same conclusion. An illustrative example of such a heteroclinic connection is given in Figure 1.
- $\alpha = -2$  : We note that, as the minimum of  $g$  now occurs at  $u_{min} = -1$ , we no longer have our desired  $u_p \neq -1$  such that  $g(u_p) = -1$ . Thus, we conclude that for a semi-infinite network, there exists no heteroclinic connection between  $-1$  and  $1$ , and so no such stationary profile exists. Interestingly, we still have the existence of such a connection, and thus a stationary profile, in our bi-infinite network (one can imagine such a heteroclinic by observing Figure 1).
- $\alpha < -2$ : In our final case, we see no change in behavior from  $\alpha = -2$  in our bi-infinite network. A heteroclinic connection between  $-1$  and  $1$  still exists, and so we still have a  $-1 \rightarrow 1$  stationary profile. In the semi-infinite case,  $-1$  regains its preimage,  $u_p \neq -1$ , however, subsequent preimages of  $u_p$  fail to exist under  $g$ , and so we have no stationary profile.

■

### 3.1.3 Linear Wavespeeds

Armed with a complete understanding of conditions on  $\alpha$  which force the existence of a stationary front we now turn our attention to characterizing the speed at which invading

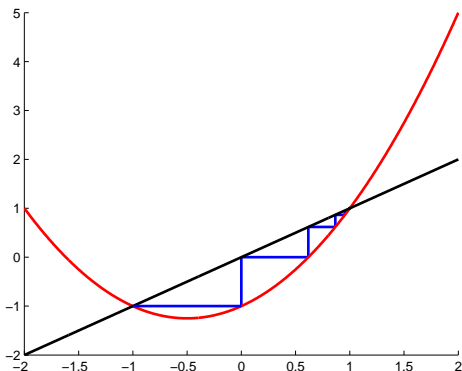


Figure 1: An example of 15 iterations under the map  $g$  when  $\alpha = -1$ . As the point  $-1$  has a preimage under  $g$ , we find a heteroclinic connection joining  $-1$  to  $1$  at  $j = \infty$ , implying the existence of a  $-1 \rightarrow 1$  stationary profile. The diagonal has been shown for illustrative purposes.

fronts propagate through our network. Recalling the discussion in Section 2.3 we deduce the dispersion relation,

$$\lambda(\sigma) = ic\sigma - 2\bar{u} + \alpha(1 - e^{-i\sigma}).$$

We then employ our double root criterion (2.12) to find

$$\lambda = -2\bar{u} + \alpha(1 - e^{-i\sigma}) + ic\sigma = 0 \tag{3.1}$$

and

$$\frac{\partial \lambda}{\partial \sigma} = \alpha i e^{-i\sigma} + ic = 0. \tag{3.2}$$

From (3.2), we find the relations

$$c = -\alpha e^{-i\sigma} \text{ and } \sigma = i \log\left(-\frac{c}{\alpha}\right),$$

which, upon substitution into (3.1), produce the equation in  $c$

$$-2\bar{u} + \alpha + c \left(1 - \log\left(-\frac{c}{\alpha}\right)\right) = 0,$$

with solution

$$c = \frac{-2\bar{u} + \alpha}{W\left(\frac{2\bar{u} - \alpha}{e\alpha}\right)}. \tag{3.3}$$

Here,  $W(x)$  denotes the Lambert W function, which is defined as the solution to

$$W(x)e^{W(x)} = x. \tag{3.4}$$

For  $-e^{-1} \leq x \leq 0$ ,  $W(x)$  will have two solutions, or branches, denoted  $W_{-1}(x)$  and  $W_0(x)$  respectively. As we will see, both of these branches will be of use later, with the  $-1$  branch corresponding to solutions of (3.4) smaller than  $-1$ , that is,  $W_{-1}(x) \leq -1$ , while all other solutions will be found on the higher,  $0$ , branch i.e.  $W_0(x) \geq -1$ . Further, this  $0$  branch will eventually become the only real solution to (3.4) when  $x > 0$  (no real solutions exist for

$x < -\frac{1}{e}$ ). While this description of the Lambert function will be sufficient for our purposes, a more detailed examination may be found in [3].

Simply setting  $\bar{u} = -1$ , we see that we will have at most two wavespeeds (shown in Figure 2), corresponding to the 0 and  $-1$  branches of  $W(x)$  respectively. The former branch will give us the speed of our leading front,  $c_0$ , i.e. the “linear speed of propagation” away from the unstable equilibrium  $-1$  discussed in Section 2.3, and is equivalent to the speed at which a stable state such as 1, will invade the unstable  $-1$ . The latter branch will respectively give us the speed,  $c_{-1}$ , of the back end of a convecting instability. The wave speed  $c_{-1}$  may then be understood as the speed of a “restoring front” which returns our network to its initial state  $-1$ , and is equivalent to the speed at which the state  $-1$  invades 1.

Examining our explicit formula for computing our wavespeeds (3.3), we see that as  $\alpha \rightarrow -2$ ,  $c_{-1} \rightarrow 0$ , our network undergoes a bifurcation from a convective to absolute instability about  $-1$ , corresponding to the bifurcations discussed by [8]. Of further interest is that this is the precise moment at which we gain the existence of a  $-1 \rightarrow 1$  stationary profile, that is, as  $\alpha \rightarrow -2$ , we see an increasingly sharp restoring wave, which eventually degenerates into a stationary profile. A visual representation of this information may be found in Figure 2.



Figure 2: The two leftmost pictures show numerical simulations of a feed-forward network with 40 cells (horizontally) over 300 time units (vertically). Black denotes the state 1, while copper denotes  $-1$ . The far left picture shows such a simulation for  $\alpha = -3$ , at which point both  $c_{-1}, c_0 \neq 0$ . Thus, we see a convecting instability. In contrast, the middle picture, a simulation with  $\alpha = -1$ , shows the propagation of an absolute instability, which remains indefinitely. The final figure shows the two analytically computed branches of (3.3), together with numerically computed, nonlinear wavespeeds shown as dots.

### 3.1.4 Wavespeed Asymptotics

Here we make use of the known asymptotic behavior of the 0 and  $-1$  branches of the Lambert  $W$  function to elucidate a first order approximation to the behavior of both  $c_0$  and  $c_{-1}$  near their respective annihilation points.

Beginning first with an examination of  $c_{-1}$ , we have from (3.3) and the preceding discussion

$$c_{-1}(\alpha) = \frac{2 + \alpha}{W_{-1}\left(\frac{-2-\alpha}{e\alpha}\right)}. \quad (3.5)$$

Setting  $x = \frac{-2-\alpha}{e\alpha}$ , we see that as  $\alpha \rightarrow -2^-$ ,  $x \rightarrow 0^-$ . Making use of the known behavior of  $W_{-1}(x)$  as  $x \rightarrow 0^-$  (see [3]), we have

$$W_{-1}(x) \sim \log(-x) \text{ as } x \rightarrow 0^-.$$

We obtain the following asymptotic for  $c_{-1}$

$$c_{-1}(\alpha) \sim \frac{2 + \alpha}{\log(-2 - \alpha)}, \text{ as } \alpha \rightarrow -2^-.$$

Now turning our attention to  $c_0$ , defined as

$$c_0(\alpha) = \frac{2 + \alpha}{W_0\left(\frac{-2 - \alpha}{e\alpha}\right)}, \quad (3.6)$$

we see upon setting  $x = \frac{-2 - \alpha}{e\alpha}$ , that as  $\alpha \rightarrow 0^-$ ,  $x \rightarrow \infty$ , and so  $W_0(x) \sim \log(x)$ . Using this information we find the asymptotic

$$c_0(\alpha) \sim -\frac{2}{\log(-\alpha)} \text{ as } \alpha \rightarrow 0^-.$$

As a closing note, we could in principle apply the same techniques discussed throughout the two previous sections to find the various wavespeeds associated with our unstable flip flop equilibrium. We choose to omit such a discussion to avoid excessive repetition.

## 3.2 Pitchfork Bifurcation

With our discussion of the fold nonlinearity now complete, we next examine  $f(u) = u(1 - u^2)$ . Here, we will repeat a similar analysis to our previous section though we will restrict our analysis to semi-infinite networks. To begin, we will address constraints on  $\alpha$  which permit the existence and stability of various equilibria and specific stationary profiles.

### 3.2.1 Existence and Stability of Equilibria

Using precisely the same methods as in the previous section, we seek to find conditions on  $\alpha$  which will permit the existence and stability of certain stationary profiles. To this end, we must first categorize the various equilibria of our system and their temporal stability.

**Lemma 3.3.** *There exist precisely three homogeneous equilibria,  $-1, 1$ , and  $0$ . There also exists up to three flip flop equilibria, given by:*

- $u_{\text{flip}_1} = \sqrt{1 + 2\alpha}$ ,  $u_{\text{flop}_1} = -\sqrt{1 + 2\alpha}$  for  $\alpha \geq -\frac{1}{2}$ ;
- $u_{\text{flip}_2} = \frac{1}{2}\sqrt{2 + 2\alpha + 2\sqrt{1 + 2\alpha - 3\alpha^2}}$ ,  $u_{\text{flop}_2} = \frac{1}{2}\sqrt{2 + 2\alpha - 2\sqrt{1 + 2\alpha - 3\alpha^2}}$   
for  $-\frac{1}{3} \leq \alpha \leq 1$ ;
- $u_{\text{flip}_3} = -\frac{1}{2}\sqrt{2 + 2\alpha - 2\sqrt{1 + 2\alpha - 3\alpha^2}}$ ,  $u_{\text{flop}_3} = -\frac{1}{2}\sqrt{2 + 2\alpha + 2\sqrt{1 + 2\alpha - 3\alpha^2}}$   
for  $-\frac{1}{3} \leq \alpha \leq 1$ .

Further, the temporal stability of these equilibria is characterized as follows:

- $\pm 1$  are stable for  $\alpha < 1$ ;
- $0$  is always unstable;
- $u_{\text{flip}_1}, u_{\text{flop}_1}$  is stable for  $\alpha > -\frac{1}{3}$ ;

- $u_{\text{flip}_k}, u_{\text{flop}_k}$  is always unstable for  $k = 2, 3$ .

In Figure 3, we show the values of all flip flop equilibria (and homogeneous equilibria) as a function of  $\alpha$ , and summarize the regions in which they are stable. Note that the value  $\alpha = -\frac{1}{3}$  is the location of the pitchfork bifurcation denoted by diamonds in Figure 3, which in turn corresponds to the loss of stability of  $(u_{\text{flip}_1}, u_{\text{flop}_1})$ .

**Proof.** The proof is identical to the proof of Lemma 3.1, and is thus omitted. ■

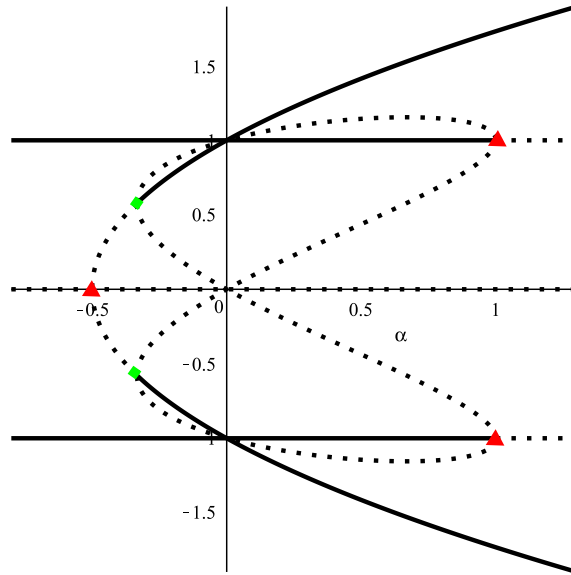


Figure 3: Bifurcation diagram in  $\alpha$ . Here, dotted lines represent temporally unstable equilibria, while solid represent temporally stable. The three horizontal lines correspond to the three homogeneous equilibria, and the remaining six curves correspond to the various flips and flops of Lemma 3.3. Specifically, the two outermost curves correspond to  $u_{\text{flip}_1}, u_{\text{flop}_1}$ . The four remaining curves give, going from highest to lowest,  $u_{\text{flip}_2}, u_{\text{flop}_2}, u_{\text{flip}_3}, u_{\text{flop}_3}$ . Triangles and diamonds represent the location of various pitchfork bifurcations, with the diamond pitchfork bifurcation being precisely the bifurcations referenced in Lemma 3.3.

### 3.2.2 Stationary Interfaces

Though the general structure of this section will be similar to that of the fold, a complete evaluation of every possible stationary profile and traveling front associated with this network would be too lengthy, and so we will avoid such an analysis. Instead, we will examine interfaces between  $0 \rightarrow 1$  and  $0 \rightarrow FF$ , where for the duration of this section, we will always assume the state FF corresponds to our flip flop equilibrium  $u_{\text{flip}_1}, u_{\text{flop}_1}$ . Further, we also note that by understanding the behavior of a  $0 \rightarrow 1$  interface, we simultaneously gain insight into interfaces of form  $0 \rightarrow -1$  thanks to the reflection symmetry of our system about 0.

**Lemma 3.4.** *In a semi-infinite network, we find that*

- A stationary profile of form  $0 \rightarrow FF$  exists provided  $\alpha_- < \alpha$ , where

$$\alpha_- = \frac{4 - 6\sqrt{3}}{23}$$

- A stationary profile of form  $0 \rightarrow 1$  exists provided  $-1 < \alpha < \alpha_+$ , where

$$\alpha_+ = \frac{4 + 6\sqrt{3}}{23}.$$

Further, a  $0 \rightarrow 1$  stationary profile exists precisely when a  $0 \rightarrow -1$  profile exists.

An illustration of these results can be found in Figure 5.

**Proof.** Recalling Remark 2.9, a stationary profile of form  $0 \rightarrow \bar{u}$  will exist precisely when there exists  $u_p \neq 0$  such that  $g(u_p) = 0$ , whose subsequent preimages under  $g$  converge to converge to  $\bar{u}$ .

- $\alpha < -1$ : Here, the point 0 ceases to have any preimage,  $u_p \neq 0$ , and so no stationary profile with state 0 at  $j = 0$  will exist.
- $-1 < \alpha < \alpha_-$ : Here we find two possible preimages of 0 which are equal in magnitude,  $\pm u_p$ . We find that the subsequent preimages under  $g$  of  $u_p$  exist and converge to 1, while those of  $-u_p$  converge to  $-1$ . Thus, we conclude the existence of a  $0 \rightarrow \pm 1$  stationary profile in this region.
- $\alpha_- < \alpha < \alpha_+$ : In this region, we find the existence of several possible heteroclinic connections to 0 at  $j = 0$ . While heteroclinic connections joining 0 and  $\pm 1$  are evident by graphical inspection (see Figure 4), the precise conditions which allow for a heteroclinic connection to flip flops are slightly more obscure. Denoting the two preimages of 0 on this interval as  $\pm u_p$ , we compute  $\alpha_-$  and  $\alpha_+$  by computing the precise moment at which there exists additional preimages of  $\pm u_p$  in addition to those used in the heteroclinic connections to  $\pm 1$ . Clearly,  $\alpha_-$  is then found by the relation  $g^{-1}(u_p) = u_{max}$  where  $u_{max}$  denotes the local maximum of  $g$  on  $(-1, 1)$ , while  $\alpha_+$  is found using  $g^{-1}(u_p) = u_{min}$ , where  $u_{min}$  denotes the local minimum of  $g$  on the same interval.
- $\alpha_+ < \alpha$ : We lose only our  $0 \rightarrow 1$  stationary profiles, as both the local maximum and minimum of  $g$  now lie in the interval  $(-1, 1)$  and so our previously discussed heteroclinic connections corresponding to these two states disappear.

■

### 3.2.3 Linear Wavespeeds

Applying precisely the same techniques used in Section 3.1.3, we find an expression for the linear wavespeeds associated with our 0 equilibrium,

$$c = \frac{1 + \alpha}{W\left(\frac{-1-\alpha}{e\alpha}\right)}. \quad (3.7)$$

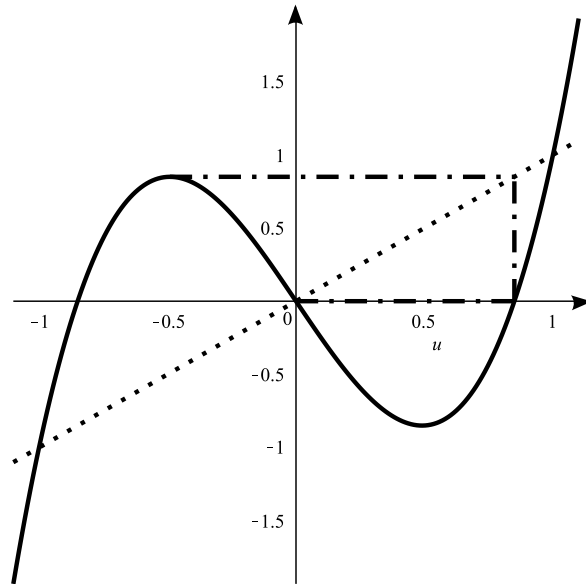


Figure 4: Preimages of 0 under  $g$  when  $\alpha \gtrsim \alpha_-$ . Here, one can imagine four possible heteroclinic connections, corresponding to the four preimages of the points  $\pm 1$ , which are themselves the two preimages of 0.

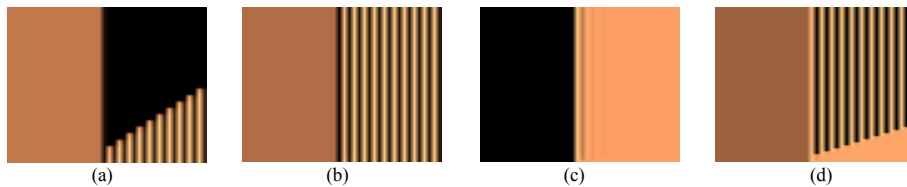


Figure 5: Numerical simulations of a semi-infinite pitchfork network using 350 time units (vertically) and 40 cells (horizontally). In (a),  $\alpha \lesssim \alpha_-$ , while in (b)  $\alpha \gtrsim \alpha_-$  and so we see the existence of a  $0 \rightarrow FF$  stationary profile only in (b). Similarly, in (c),  $\alpha \lesssim \alpha_+$ , and in (d)  $\alpha \gtrsim \alpha_+$ , and so we see a  $0 \rightarrow 1$  stationary profile in (c), but not in (d).

In accordance with our earlier results, we see that for  $\alpha < -1$ , equation (3.7) has two solutions,  $c_{-1}$  and  $c_0$ , corresponding to the  $-1$  and  $0$  branches of our solution respectively. When  $\alpha = -1$ , i.e. at the moment at which we gain the existence of a  $0 \rightarrow 1$  stationary profile,  $c_{-1}$  becomes  $0$ , and the propagation of our instability becomes absolute as opposed to convective. Finally, as  $\alpha \rightarrow 0$ ,  $c_0 \rightarrow 0$ , at which point a frustrated front emerges, and instabilities about  $0$  no longer propagate through our network. Noting that (3.7) is functionally identical to (3.3), we obtain precisely the same asymptotic behavior for  $c_{-1}$  and  $c_0$  near their annihilation points. That is

$$c_{-1} \sim \frac{1 + \alpha}{\log(-1 - \alpha)} \quad \text{as } \alpha \rightarrow -1^-,$$

and

$$c_0 \sim \frac{-1}{\log(-\alpha)} \quad \text{as } \alpha \rightarrow 0^-.$$

## 4 Cusp

Keeping the methods and results of the previous sections in mind, we now move to study our final nonlinear dynamics, which will now mimic a rescaled cusp bifurcation with codimension 2. Throughout this section, we will work with the following cubic nonlinearity  $f(u) = u(1 - u)(u - a)$ , where we will restrict to  $0 < a < \frac{1}{2}$ .

The remainder of this section is organized as follows. We begin with a discussion of the various period-two equilibria of our system, which we will take throughout this section to be of semi-infinite length. We will then describe various stationary profiles which exist in our network. During this discussion, we will see that for our semi-infinite network the unique dynamics of our  $j = 0$  cell given from (1.1) will play an important role in the characterization of certain stationary profiles.

### 4.1 Existence and Stability of Equilibria

Here, we discuss all period-two equilibria of (1.1) and their stability, the results of which are summarized in Figures 6 and 7. We will drop the Lemma-Proof nature of the previous sections, and instead give a more general overview of the methods used to construct the previously mentioned figures. In general, the values and stability of our equilibria shown in Figure 6 have been computed numerically by solving system (2.5) and examining the eigenvalues associated with the linearization of (2.5) about the equilibria in question.

Since finding the homogeneous equilibria of our system remains a trivial task, we immediately find the existence of three homogeneous equilibria,  $0$ ,  $a$ , and  $1$ . We find explicit relations between  $a$  and  $\alpha$  which impart temporal stability to our equilibria, which are summarized below.

- $0$  is temporally stable provided  $\alpha < \frac{a}{2}$ ;
- $a$  is always temporally unstable, though as  $\alpha$  increases past  $\alpha = \frac{a^2 - a}{2}$ , the period-two Morse index of this equilibrium changes from 1 to 2;
- $1$  is temporally stable provided  $\alpha < \frac{1 - a}{2}$ ;

Of particular importance are the points in  $(a, \alpha)$  space at which our various homogeneous equilibria lose their temporal stability (or when the Morse index of our equilibria changes). These are precisely the points associated with the locations of the pitchfork bifurcations shown in Figure 6, and the lines in Figure 7. These bifurcation points will further correspond precisely to the bounds of existence for the flip flop equilibria.

We find in addition to our homogeneous equilibria up to three flip flops. Lacking an explicit expression for the values of these equilibria, we will simply describe them in terms of the curves in Figure 6 as follows:

- Our first flip flop equilibrium,  $u_{\text{flip}_1}, u_{\text{flip}_1}$ , corresponds to the two outermost curves (the lower of which will correspond to  $u_{\text{flip}_1}$ , the higher to  $u_{\text{flip}_1}$ ). This flip flop is temporally stable over its entire interval of existence,  $\alpha_{\text{saddle}}(a) < \alpha$ , where  $\alpha_{\text{saddle}}(a)$  denotes the location of the saddle-node bifurcation in our system. In future sections, any stationary interface using the symbol  $FF$  will refer to this equilibrium.
- We define  $u_{\text{flip}_2}, u_{\text{flip}_2}$  to be the equilibrium given by the two lower curves, which are always temporally unstable, and exist for  $\frac{a^2-a}{2} < \alpha < \frac{a}{2}$ .
- Our final flip flop equilibrium  $u_{\text{flip}_3}, u_{\text{flip}_3}$  corresponds to the two remaining curves, and is always unstable. It exists for  $\alpha_{\text{saddle}}(a) < \alpha < \frac{1-a}{2}$ .

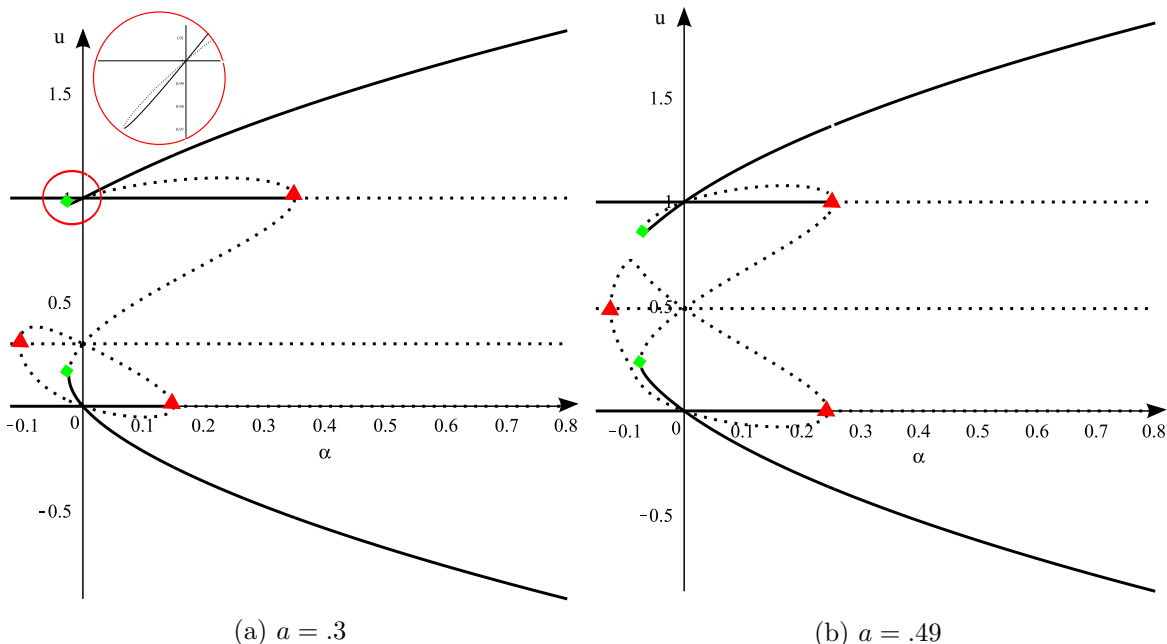


Figure 6: Bifurcation diagram in the  $(a, \alpha)$  plane of the period-two equilibria of our system. Similarly to Figure 3, dotted lines represent temporally unstable equilibria, while solid represent stable equilibria. Triangles correspond to the pitchfork bifurcations associated with our homogeneous equilibria, and diamonds correspond to the saddle node bifurcation. Observe that, at  $a = \frac{1}{2}$  we recover Figure 3.

To complete the picture, it now remains to describe how we computed the previously mentioned  $\alpha_{\text{saddle}}(a)$ , the location of the saddle node bifurcation from which our first flip flop

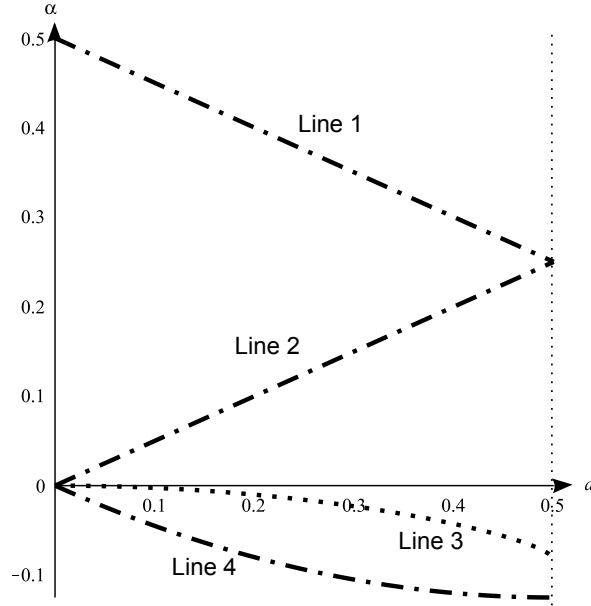


Figure 7: Locations of the various bifurcations in the  $a - \alpha$  plane. Here, Line 1 =  $\frac{1}{2}(1 - a)$  corresponds to the location of the pitchfork bifurcation associated with the homogeneous equilibrium 1. Line 2 =  $\frac{a}{2}$  corresponds to the pitchfork associated with 0. Line 3 shows  $\alpha_{saddle}(a)$ . Line 4 =  $\frac{a^2 - a}{2}$  gives the location of our final pitchfork bifurcation, associated with the equilibrium  $a$ .

equilibrium emerges. To this end we note that upon adding, and respectively subtracting, the nullclines corresponding to equations (2.5), we find

$$f(u_0) + f(u_1) = 0, \tag{4.1a}$$

$$\frac{f(u_0) - f(u_1)}{u_0 - u_1} = -2\alpha. \tag{4.1b}$$

With these equations in mind, we set  $u_0 = u_{\text{flip}_1}, u_1 = u_{\text{flip}_1}$ , and will now make use of a geometric intuition to find the location of our saddle node. From Figure 6, we see that for  $\alpha$  large,  $u_{\text{flip}_1} \gg 0$  while  $u_{\text{flip}_1} \ll 0$ . As  $\alpha$  decreases, we see that  $u_{\text{flip}_1}$  briefly becomes 0 precisely as  $u_{\text{flip}_1}$  becomes 1. Finally, as  $\alpha$  continues to decrease,  $u_{\text{flip}_1}$  attains its minimum value just as  $u_{\text{flip}_1}$  attains its maximum value.

Keeping this information in mind we then turn our attention to Figure 8. From (4.1), we see that the images under  $f$  of  $u_{\text{flip}_1}$  and  $u_{\text{flip}_1}$  must be equal but opposite in sign. Starting at  $\alpha = 0$ , i.e. when  $u_{\text{flip}_1} = 0$  and  $u_{\text{flip}_1} = 1$  and slowly decreasing  $\alpha$ , we see that the slope of the secant line between our two points must become slowly more positive, attaining its maximum precisely at the location of our saddle node. By visual inspection, we see that this occurs precisely when

$$u_{\text{flip}_1} = \frac{1 + a - \sqrt{a^2 - a + 1}}{3} = u_{\text{min}},$$

where  $u_{\text{min}}$  denotes the minimum of  $f$  on the interval  $(0, 1)$ . This constraint may then be used in conjunction with (4.1) to produce a relation  $\alpha_{saddle}(a)$ , giving the location of our saddle node bifurcation for all  $a$ .

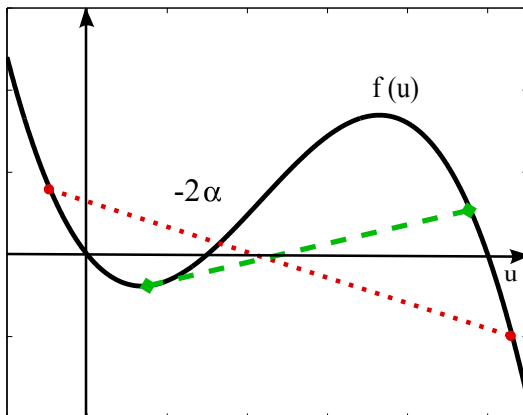


Figure 8: Illustrative example using the geometric argument for computing  $\alpha_{saddle}(a)$ . Each secant line joints the image of  $u_{flip_1}$  with that of  $u_{flip_1}$  under  $f$ . We see that the red dotted line, which has negative slope, corresponds to positive  $\alpha$ , while the green dash-dot line with positive slope corresponds to  $\alpha$  negative.

## 4.2 Stationary Profiles

Having looked at the stability of our equilibria, we now analyze existence conditions of stationary interfaces of forms  $0 \rightarrow FF$ ,  $1 \rightarrow FF$ ,  $0 \rightarrow 1$ ,  $1 \rightarrow 0$ ,  $FF \rightarrow 1$ ,  $FF \rightarrow 0$ , and  $FF \rightarrow FF'$ . Here  $FF \rightarrow FF'$  designates a cell system of flip flops with a defect, e.g. a system that goes flip flop flip flop or flop flip flop flop flip. Similarly to previous sections, we make use of Remark 2.9 to establish boundaries in the  $a, \alpha$  in which heteroclinics, and thus stationary profiles, exist between our two states in question. While the tedious details of this analysis will not be given here, upon inspecting the map in detail, one can in fact verify that our boundaries are sharp. Our results are given in Figure 9 and Table 1. In the following section, we compare these predictions to numerical results.

To illustrate those results, consider Regions 1 and 2. In Region 1, Table 1 shows that there exist only two stationary interfaces,  $0 \rightarrow FF$  and  $1 \rightarrow FF$ . We now examine changes as we cross the boundary from Region 1 into Region 2. Referencing Table 1 and looking at both the rows for Region 1 and Region 2, we see that the only change is for the interface  $0 \rightarrow 1$ , which exists in Region 2 but not in Region 1. One can examine all region boundaries in this fashion, obtaining a complete bifurcation diagram for stationary interfaces.

**Remark 4.1.** *We find that only the boundary between Region 5 and Region 8 and the boundary between Regions 6 and 7 can be expressed explicitly as  $-(\frac{a}{2})^2$  and  $-(\frac{1-a}{2})^2$ , respectively. In fact, Regions 8 and 9 are subregions of Regions 6 and 7, respectively. In these subregions, the same behavior is observed for the interfaces  $0 \rightarrow 1$ ,  $1 \rightarrow 0$ ; however, since stable flip flops still exist in these subregions we distinguish them as separate regions in order to examine the interfaces  $0 \rightarrow FF$ ,  $1 \rightarrow FF$ ,  $FF \rightarrow 1$ ,  $FF \rightarrow 0$ , and  $FF \rightarrow FF'$ . The line specifying the boundary between each of these regions and their subregions is given by the flip flop saddle node.*

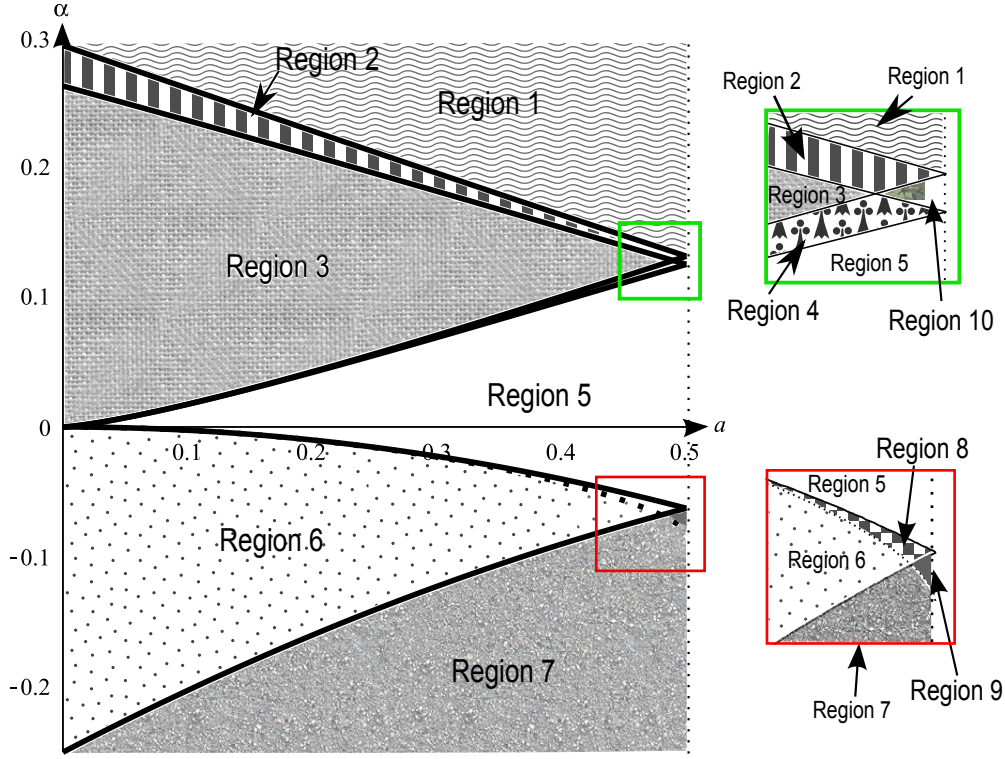


Figure 9: Each solid line expresses  $\alpha$  as a function of  $a$  and each one represents the upper bounds for the existence of a stationary interface. The dotted line expresses the value of  $\alpha$  for which a saddle node bifurcation occurs. For each region the existence of a given interface can be found in Table 1.

Region	$0 \rightarrow FF$	$1 \rightarrow FF$	$0 \rightarrow 1$	$1 \rightarrow 0$	$FF \rightarrow 1$	$FF \rightarrow 0$	$FF \rightarrow FF'$
1	X	X	N	N	N	N	N
2	X	X	X	N	N	N	N
3	X	X	X	N	X	N	X
4	X	X	X	X	X	N	X
5	X	X	X	X	X	X	X
6	NA	NA	X	N	NA	NA	NA
7	NA	NA	N	N	NA	NA	NA
8	X	N	X	N	T	T	T
9	N	N	N	N	T	T	N
10	X	X	X	X	N	N	N

Table 1: Existence of stationary interfaces: X indicates that the stationary interface exists, N indicates that the stationary interface does not exist, NA indicates that we cannot examine the interface because stable flip flops no longer exist in the region, and T indicates that the stationary interface exists in the infinite but possibly not in the semi-infinite lattice; see Section 4.4 for more details on this case.

### 4.3 Numerical Simulations

In this section, we display numerical simulations exhibiting interface dynamics for various regions of Figure 9. These simulations confirm that the necessary information gathered in Figure 9 and Table 1 give sharp criteria. In all the simulation figures of this section the notation  $R_A/R_B$  specifies that we are looking at region  $A$  near region  $B$ . Time is increasing vertically, and the horizontal axis of each picture is the cell index  $j$  where  $1 \leq j \leq 40$ . In addition, for all simulation figures lighter colors correspond to values near 1, while darker colors correspond to values near 0. Note however that the color scaling is not uniform across figures.



Figure 10: (a):  $R_1, 1 \rightarrow FF$ ,  $a = 0.3$ ,  $\alpha = 0.197$ , and  $t = 300$  units. (b):  $R_1, 0 \rightarrow FF$ ,  $a = 0.3$ ,  $\alpha = 0.197$ , and  $t = 300$  units. (c):  $R_1/R_2, 0 \rightarrow 1$ ,  $a = 0.3$ ,  $\alpha = 0.197$ , and  $t = 300$  units. (d):  $R_2/R_1, 0 \rightarrow 1$ ,  $a = 0.3$ ,  $\alpha = 0.192$ , and  $t = 300$  units.



Figure 11: (a):  $R_2/R_3, FF \rightarrow 1$ ,  $a = 0.3$ ,  $\alpha = 0.183$ , and  $t = 800$  units. (b):  $R_3/R_2, FF \rightarrow 1$ ,  $a = 0.3$ ,  $\alpha = 0.18$ , and  $t = 300$  units. (c):  $R_2/R_3, FF \rightarrow FF'$ ,  $a = 0.3$ ,  $\alpha = 0.183$ , and  $t = 800$  units. (d):  $R_3/R_2, FF \rightarrow FF'$ ,  $a = 0.3$ ,  $\alpha = 0.18$ , and  $t = 300$  units.

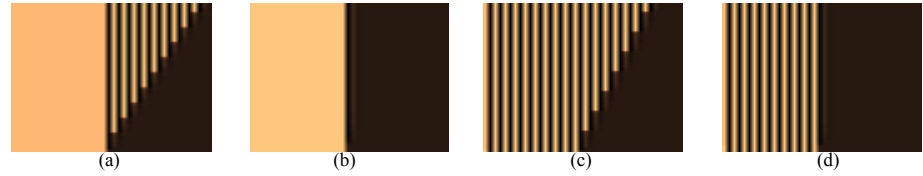


Figure 12: (a):  $R_3/R_4, 1 \rightarrow 0$ ,  $a = 0.3$ ,  $\alpha = 0.072$ , and  $t = 800$  units. (b):  $R_4/R_3, 1 \rightarrow 0$ ,  $a = 0.3$ ,  $\alpha = 0.07$ , and  $t = 300$  units. (c):  $R_4/R_5, FF \rightarrow 0$ ,  $a = 0.3$ ,  $\alpha = 0.07$ , and  $t = 1000$  units. (d):  $R_5/R_4, FF \rightarrow 0$ ,  $a = 0.3$ ,  $\alpha = 0.068$ , and  $t = 300$  units.

### 4.4 Effects of Truncation

In this section we will briefly discuss the effects of the  $0^{th}$  cell in a semi-infinite system and discuss Figure 16. More precisely, upon examining (1.1) one can see that if the  $0^{th}$  cell is initialized to  $u_*$  such that  $f(u_*) \neq 0$ , the cell will change in value until equal to the nearest homogeneous equilibrium  $\bar{u}$ , e.g. 1 or 0.

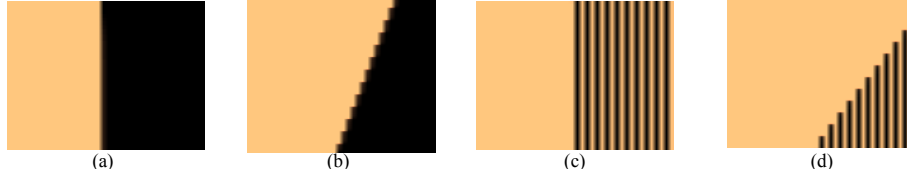


Figure 13: (a):  $R_5/R_8$ ,  $1 \rightarrow 0$ ,  $a = 0.3$ ,  $\alpha = -0.022$ , and  $t = 300$  units. (b):  $R_8/R_5$ ,  $1 \rightarrow 0$ ,  $a = 0.3$ ,  $\alpha = -0.023$ , and  $t = 2000$  units. (c):  $R_5/R_8$ ,  $1 \rightarrow FF$ ,  $a = 0.3$ ,  $\alpha = -0.022$ , and  $t = 300$  units. (d):  $R_8/R_5$ ,  $1 \rightarrow FF$ ,  $a = 0.3$ ,  $\alpha = -0.023$ , and  $t = 1500$  units.



Figure 14: (a):  $R_8/R_6$ ,  $1 \rightarrow 0$ ,  $a = 0.3$ ,  $\alpha = -0.022$ , and  $t = 2000$  units. (b):  $R_6/R_8$ ,  $1 \rightarrow 0$ ,  $a = 0.3$ ,  $\alpha = -0.024$ , and  $t = 1500$  units. (c):  $R_6/R_7$ ,  $0 \rightarrow 1$ ,  $a = 0.3$ ,  $\alpha = -0.121$ , and  $t = 300$  units. (d):  $R_7/R_6$ ,  $0 \rightarrow 1$ ,  $a = 0.3$ ,  $\alpha = -0.124$ , and  $t = 2000$  units.

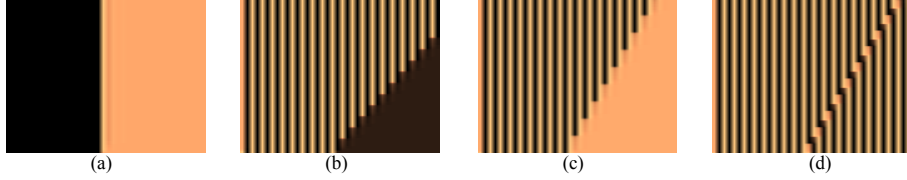


Figure 15: (a):  $R_{10}$ ,  $0 \rightarrow 1$ ,  $a = 0.496$ ,  $\alpha = 0.128$ , and  $t = 300$  units. (b):  $R_{10}$ ,  $FF \rightarrow 0$ ,  $a = 0.496$ ,  $\alpha = 0.128$ , and  $t = 800$  units. (c):  $R_{10}$ ,  $FF \rightarrow 1$ ,  $a = 0.496$ ,  $\alpha = 0.128$ , and  $t = 800$  units. (d):  $R_{10}$ ,  $FF \rightarrow FF'$ ,  $a = 0.496$ ,  $\alpha = 0.128$ , and  $t = 1500$  units.

In numerical simulations, we expect a stationary  $FF \rightarrow A$  interface in certain regions, though these interfaces may in fact appear to be non-stationary when studied in a semi-infinite lattice (see the entries 'T' of Table 1). This can be explained by the behavior of the  $0^{th}$  cell creating a new interface which may be non-stationary. For example, in Region 8 of Figure 9, one would expect the  $FF \rightarrow 1$  interface to be stationary; however, if the  $0^{th}$  cell of the  $FF$  cluster is initialized to the flip, the interface will appear non-stationary because the  $0^{th}$  cell goes from a value of *flip* to a value of 1 creating a  $1 \rightarrow FF$  interface which is non-stationary as seen in Table 1. This causes an invasion front to propagate through the system during the simulation making the original interface appear non-stationary.

In Figure 16, (a) and (e) illustrate the effect of the  $0^{th}$  node on a  $FF \rightarrow FF'$  interface. They also show how the two different  $FF \rightarrow FF'$  interfaces possess different properties. Figures (b), (c), and (d) all demonstrate boundary effects on the  $FF \rightarrow 0$  interface. In Region 8, an effect similar to (c) occurs, but is omitted here. Similarly, (f), (g), and (h) demonstrate the boundary effects on the  $FF \rightarrow 1$  interface. Again in Region 8 an effect similar to (g) occurs, but is omitted here. On the other hand, figures (d) and (h) showcase effects unique to Region

9, whose their corresponding counterparts in Region 8 are shown in (b) and (f), respectively.

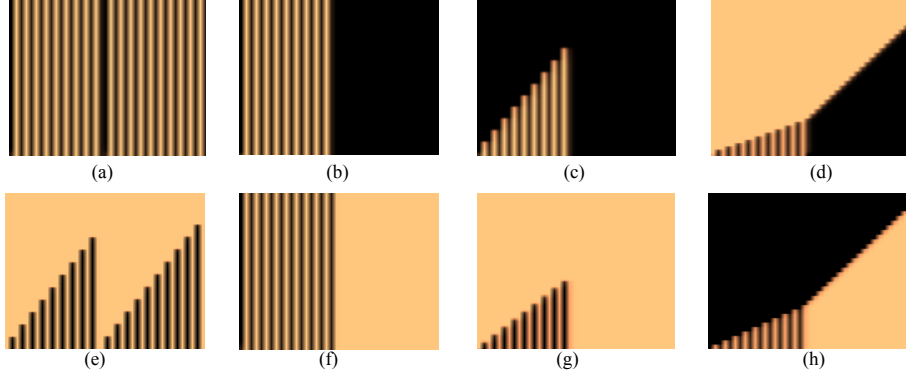


Figure 16: (a):  $R_8, FF \rightarrow FF'$ ,  $a = 0.3$ ,  $\alpha = -0.023$ , and  $t = 300$  units. (b):  $R_8, FF \rightarrow 0$ ,  $a = 0.3$ ,  $\alpha = -0.023$ , and  $t = 300$  units. (c):  $R_9, FF \rightarrow 0$ ,  $a = 0.493$ ,  $\alpha = -0.069$ , and  $t = 800$  units. (d):  $R_9, FF \rightarrow 0$ ,  $a = 0.493$ ,  $\alpha = -0.069$ , and  $t = 1500$  units. (e):  $R_8, FF \rightarrow FF'$ ,  $a = 0.3$ ,  $\alpha = -0.023$ , and  $t = 1500$  units. (f):  $R_8, FF \rightarrow 1$ ,  $a = 0.3$ ,  $\alpha = -0.023$ , and  $t = 1500$  units. (g):  $R_9, FF \rightarrow 1$ ,  $a = 0.493$ ,  $\alpha = -0.069$ , and  $t = 800$  units. (h):  $R_8, FF \rightarrow 1$ ,  $a = 0.493$ ,  $\alpha = -0.069$ , and  $t = 2000$  units.

## 5 Discussion

Here we have studied coherent structures in feed-forward chains quite systematically. We expect that our results can be easily adapted to other nonlinearities  $f$ . While our previously discussed “toy nonlinearities” are motivated by simple normal forms at individual lattice sites, it would be interesting to obtain these normal forms in a more systematic way using ideas from [9].

On the other hand, it would be interesting to explore more complicated cell dynamics. We expect some of our results to survive quite literally. For instance, we expect that bifurcations in finite lattices can still be viewed as transitions from convective to absolute instabilities, corresponding to the formation of infinitely steep, frustrated invasion fronts. Further, we expect that in certain cases these complex systems may still be understood through their spatial dynamics in  $j$ , i.e. by reduction to interval maps. As an example, we mention excitable dynamics,

$$\begin{aligned}\dot{u}_j &= f(u_j) - v_j + \alpha(u_j - u_{j-1}), \\ \dot{v}_j &= \varepsilon(u_j - \gamma v_j),\end{aligned}$$

where stationary interfaces solve a simple scalar recursion after substituting  $v_j := u_j/\gamma$  into  $f(u_j) - v_j + \alpha(u_j - u_{j-1}) = 0$ . One can then study the effects of front pinning on excitation pulses in a systematic fashion.

Similarly, Hopf normal form dynamics

$$\dot{u}_j = u_j f(|u_j|^2) + \alpha(u_j - u_{j-1}), \quad u_j \in \mathbb{C},$$

can be reduced to iterations for  $|u_j| \in \mathbb{R}$ , choosing relative phase shifts  $\arg(u_j - u_{j-1})$  appropriately.

## 6 Acknowledgments

This research was conducted during Summer 2014 in the REU: Complex Systems at the University of Minnesota Department of Mathematics, funded by the National Science Foundation (DMS-1311414) and (DMS-1311740); see (<http://math.umn.edu/~gfaye/reu.html>).

## References

- [1] A.N. Bers. Space-time evolution of plasma instabilities - absolute and convective. *In: Rosenbluth, M.N., Sagdeev, R.Z. (eds.), Handbook of Plasma Physics*, 1983.
- [2] A. Couairon and J-M. Chomaz. Absolute and convective instabilities, front velocities and global modes in nonlinear systems. *Physica D*, 108, pp. 236–276, 1997.
- [3] R.M. Corless, G.H. Gonnet, D.E.G. Hare, D.J. Jeffrey and D.E. Knut. On the Lambert  $W$  function. *Advances in Computational Mathematics*, 5, pp 329–359, 1996.
- [4] R. Goh and A. Scheel. Triggered fronts in the complex Ginzburg-Landau equation. *J. Nonlinear Sci.*, 24, issue 1, pp. 117–144, 2014.
- [5] M. Golubitsky and I. Stewart. Nonlinear dynamics of networks: the groupoid formalism. *Bull. Amer. Math. Soc.*, 43, pp. 305–364, 2006.
- [6] A. Hoffman and B. Kennedy. Existence and uniqueness of traveling waves in a class of unidirectional lattice differential equations. *DCDS-A*, 30, pp. 137–167, 2011.
- [7] M. Holzer and A. Scheel. Criteria for Pointwise Growth and Their Role in Invasion Processes. *J. Nonlinear Sci.*, 24, issue 4, pp. 661–709, 2014.
- [8] B. Rink and J. Sanders. Amplified Hopf bifurcations in feed-forward networks. *SIAM J. Appl. Dyn. Syst.*, 12, pp. 1135–1157, 2013.
- [9] B. Rink and J. Sanders. Coupled cell networks: semigroups, Lie algebras and normal forms. *Trans. Amer. Math. Soc.*, in press, (2014).
- [10] W. van Saarloos. Front propagation into unstable states. *Physics Reports*, 386, pp 29–222, 2003.
- [11] B. Sandstede and A. Scheel. Absolute and convective instabilities of waves on unbounded and large bounded domains. *Physica D*, 145, pp. 233–277, 2000.